

# Adaptive Optics Calibration for a Wide-Field Microscope

Janice Castillo\* and Thomas Bifano

Boston University Photonics Center, 8 Saint Mary's Street, Boston, MA, USA 02215

## ABSTRACT

Adaptive optics calibration of a novel wide-field scanning microscope is described, comparing relevant parameters for several optimization techniques. Specifically, comparisons of the optimization algorithm, image quality metrics, and the calibration image target are detailed. It is shown that stochastic parallel gradient descent (SPGD) algorithm using image intensity as a metric provides robust, repeatable system optimization. Results also show that optimization performance improves when the feature sizes on the calibration target approach the diffraction limit and are more uniformly distributed. This paper further compares stochastic, image-based optimization performance to that of conventional adaptive optics optimization with a point source object and a Shack Hartmann wavefront sensor.

**Keywords:** MEMS, adaptive optics, deformable mirrors, optimization, microscopy

## 1. INTRODUCTION

The Adaptive Scanning Optical Microscope (ASOM, Thorlabs, Inc.) is a new type of microscope that enables a large viewing field at high resolution. The ASOM creates a mosaic image at high speed by through the use of a fast steering mirror (FSM, Optics in Motion, Inc.) that redirects the optical path through a scanning lens assembly (SLA). The ASOM images a sub-field-of-view at each scanned location, as illustrated in Figure 1. The sub-fields or "tiles" are then stitched together to create a large, high resolution image. This is accomplished without translation of the sample, which is beneficial when viewing several objects where relative distance is critical. It offers a field of view (FOV) up to 40mm in diameter with a resolution of 1.5  $\mu$ m. The SLA serves as a compound objective lens. The FSM selects the portion of the object to be illuminated and directs the light through the system. Many tiles in the mosaic are imaged using an optical path that does not pass through the objective's optical axis, and off-axis aberrations the SLA contribute to distortion of the those tile images. To compensate for these aberrations, the pupil of the SLA is re-imaged to a MEMS deformable mirror (DM, Boston Micromachines, Inc.). The DM is controlled in open loop to achieve a previously determined "calibration" shape that reduces the optical aberrations of that particular tile before re-imaging the pupil to the microscope's camera objective lens. This paper concentrates primarily on the efficient and robust approaches to optimizing the calibration shape used with each subaperture path through the SLA. Detailed descriptions of the ASOM have been published by Potsaid, et al [1].

The DM consists of a continuous membrane with 140 electrostatic actuators. For the DM to compensate the aberrations of a given image tile, suitable actuator commands (hereafter called the *command vector*) for the DM must be determined. It is possible to estimate the off-axis optical aberrations expected with the compound SLA as a guide to DM control for a given tile image, but manufacturing and assembly tolerances limit the effectiveness of this approach. Instead, in this paper we report on empirical approaches to calibration of the ASOM to find suitable command vectors using closed-loop optimization routines. The resulting command vectors are then stored for future use. Each image optimization routine consists of the following process: 1) A tile is selected, and the resulting image's quality is evaluated. 2) The command vector for the DM is perturbed to affect the optical wavefront (and consequently the image quality). 3) The image quality is evaluated again, and the resulting improvement or degradation of the image is used as feedback to update the command vector. This control loop continues until the image quality reaches a steady-state value.

Three questions relevant to this approach include: How do we perturb the DM command vector? How do we assess an image quality? How do features of the object or calibration target affect the overall performance? In the following sections, our efforts to answer these questions are described. The work is divided into three sections: 1) the control

---

\* jrcastle@ieee.org, 617-353-9961

technique, 2) the image quality metric, and 3) the calibration target. In the technique section, two approaches are compared: one in which the perturbations to the command vector are comprised of a series of Zernike polynomial shapes applied to the DM and one in which the perturbations to the command vector are applied to individual actuators in a stochastic, parallel gradient descent algorithm. In the metric section, image intensity and spatial frequency content are evaluated, and compared as candidate measures of image quality. In the calibration target section, the effect of symmetry and size of target object features on optimization is evaluated.

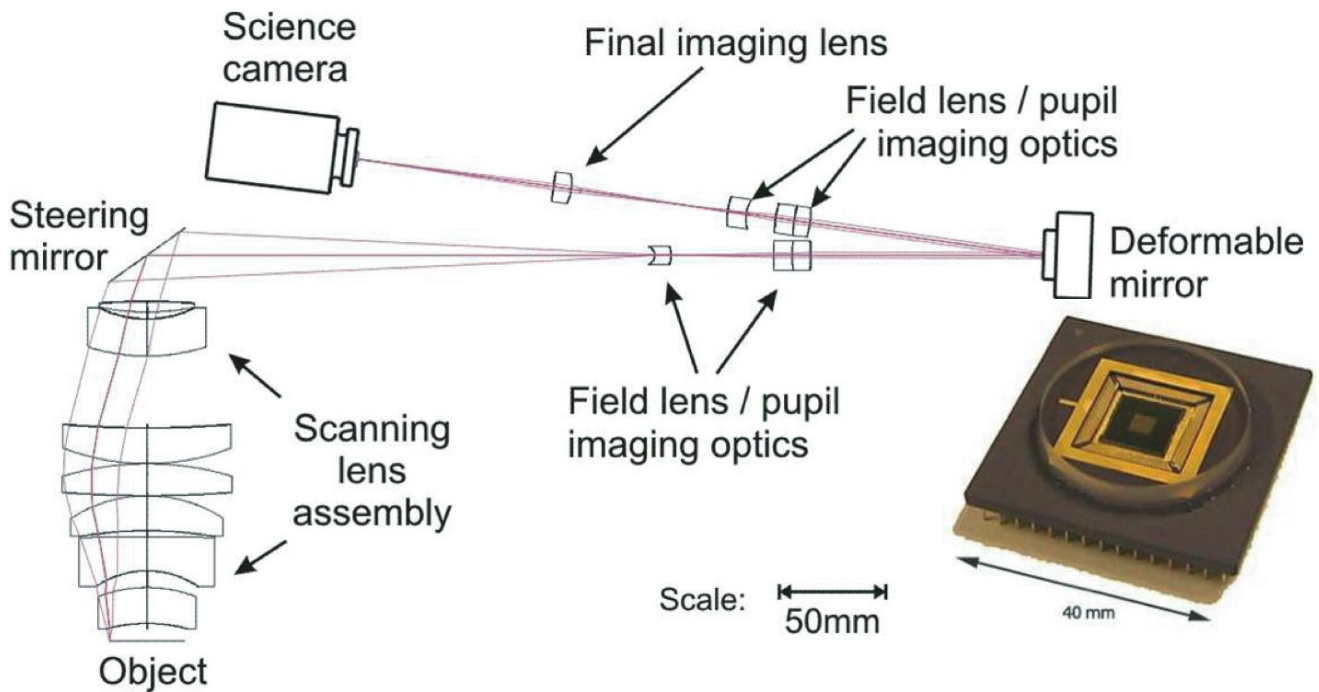


Figure 1: ASOM schematic. The instrument is a wide field-of-view microscope that uses a large diameter objective scanning lens, a fast steering mirror, and a deformable mirror to create high resolution images. The DM compensates for off-axis aberrations of the objective lens.

## 2. OPTIMIZATION METHODOLOGY

### 2.1 Control Technique

The calibration algorithms studied all comprise a multi-output, single-input controller with an unknown response. The outputs are commands to the deformable mirror, which has 140 degrees of freedom associated with its independently addressable actuators. Each actuator, in turn, can be energized to one of 256 states through digital commands to the DM driver. The single input to the system is the variable of primary interest: quality of the image. In all cases described in this work, image quality is assessed through some numerical process applied to a digitally captures image, resulting in a scalar value. No attempt is made to establish a model linking input to output. Rather, a well known stochastic control technique is used to optimize image quality in an iterative feedback control process.

To maximize calibration speed and thus the optimization speed, it is beneficial to reduce the degrees of freedom of variables in an algorithm so those that will most directly affect image quality. As already mentioned, in this work the DM has a physical construction that provides 140 degrees of freedom. One can restrict the number of achievable surface shapes by coordinating commands to actuators in an spatially organized way, reducing the effective degrees of freedom for the DM. One well-known set of shapes used in the optics field are Zernike polynomials [2]. In this work we study the

affects of applying commands that correspond to the first 36 Zernike polynomial shapes, versus applying commands to the DM actuators independently. Zernike polynomials consist of terms that have an advantage in this application: lower order terms are among those typically seen in off-axis aberrations of compound lenses (e.g. astigmatism, coma, spherical aberration).

Stochastic parallel gradient descent (SPGD) is an optimization technique pioneered in adaptive optics by Vorontsov et al for high-resolution wavefront correction [3]. Application of the algorithm is straightforward. At time step  $n$ , each element in the command vector  $C_n$  is perturbed (designated +) simultaneously by a unit amount  $\delta_n$  in a *random* direction  $+r_n$ , and then each element is perturbed (designated -) simultaneously by a unit amount  $\delta_n$  in the *opposite* direction,  $-r_n$ . After each perturbation a scalar measure of image quality  $Q_n$  is obtained. The command vector is updated based on the gradient in the quality metric. The algorithm can be expressed simply as:

- perturb  $C_n$  +, measure  $Q_n^+$ .
- perturb  $C_n$  -, measure  $Q_n^-$ .
- update the command vector  $C_{n+1} = C_n + k \delta_n r_n (Q_n^+ - Q_n^-)$

where  $k$  is a gain factor. Improved convergence rates for time-invariant aberrations have been achieved using this method by shrinking the perturbation step size with time:

$$\delta_n = \tau \delta_0 / (\tau + n) \quad (1)$$

## 2.2 Image Quality Metric

For optimization, it is necessary to have a metric that measures image quality. The metric should change monotonically with quality. Two definitions of image quality are compared in this work: cumulative intensity of the image and amplitude of high spatial frequencies in the image. The cumulative intensity metric is given by:

$$Q = \sum_A I_{xy} \quad (2)$$

where  $I_{xy}$  is the image intensity at pixel position  $x,y$  on the CCD imaging camera. This metric is sensitive to scatter and noise, but can be improved by using a power-law sum that amplifies the high-intensity values most associated with image sharpness [4]:

$$Q = \sum_A (I_{xy})^m \quad (3)$$

where  $m > 1$ . The experiments in this paper implemented the power-law metric with  $m=4$ .

An alternative way to measure image quality is to quantify image content at high spatial frequencies, since the presence of uncorrected low order aberrations tends to attenuate high spatial frequencies in the image [5,6]. This quality metric  $Q$  can be estimated by evaluating normalized image intensity after subjecting the image to a high-pass filter:

$$Q = \frac{\sum_A (I_{x,y} * F)}{\sum_A (I_{x,y})} \quad (4)$$

where  $F$  is the filter function.

## 2.3 Calibration Target

Image optimization algorithms are often tested using a USAF standard resolution test pattern. This target consists of a series of horizontal and vertical bars of various sizes. One disadvantage of this target for wide field imaging is that the

pattern of the calibration target is non-uniform, and the smallest features of the target are localized in a relatively small region. A second disadvantage is that the image's total intensity or high spatial frequency content depends strongly on the portion of the target that falls within the microscope's current field of view (i.e. the sub-image tile). As a result, it is possible that a lateral shift of the target due to image tip-tilt will change measured image quality, even though such tip and tilt should not affect image quality. A better calibration target would contain uniformly distributed features sized near the diffraction limit for the imaging system. Such targets were manufactured and tested in this work.

### 3. RESULTS

#### 3.1 Zernike control vs. independent actuator control

Figure 2 illustrates the optimization results achieved for the two algorithms tested: using gradient descent control based on Zernike shape control vectors and using gradient descent control based on independent actuator control vectors. Both methods improve the image quality, but the actuator based algorithm consistently achieves better results. One possible explanation for the disparity is that the Zernike based controller requires the DM's physical pupil to be conjugate to the microscope's imaging pupil. Even small lateral misalignments or pupil size differences will adversely affect controller performance since the control vector in Zernike-based control is defined with reference to an optical axis and a pupil diameter.

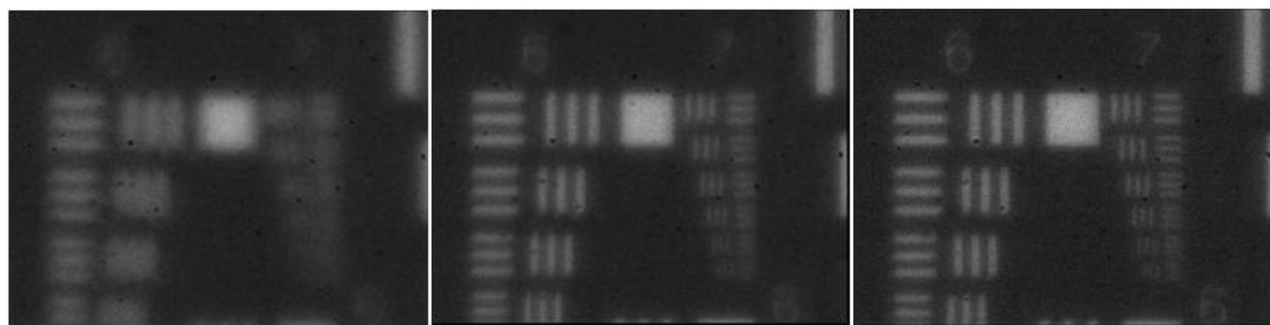


Figure 2: Characteristic end-point image quality achieved for two different gradient descent control approaches. *Left:* Image before correction, blurred by aberrations of the scanning lens. *Center:* Corrected image, Zernike-based gradient descent control. *Right:* Corrected image, actuator-based gradient descent control.

#### 3.2 Intensity metric vs. spatial frequency metric

Both intensity and spatial frequency metrics were compared using the actuator-based SPGD algorithm. The spatial filtering approach used a Laplacian-type filter designed to amplify image spatial frequencies centered at about one third of the maximum spatial frequency detectable by the CCD. Three optimization trials were performed with each of the two metrics. The average quality metric for each of the three routines are plotted in Figure 3 as a function of controller iteration. (Note: quality units are arbitrary, and lower, more negative values are indicative of improved image quality). The metric based on the summation of fourth power of measured intensity (Eqn. 3) consistently converged more rapidly than the metric based on high spatial frequency filtering (Eqn. 4). Figure 3 also illustrates the final image achieved using the intensity metric after 1500 iterations. Inspection of the calibrated target image indicates that the that the resolution of the system is between  $1.38\mu\text{m}$  and  $1.55\mu\text{m}$ . This is within a factor of two of the theoretical diffraction limited resolution for this optical system.

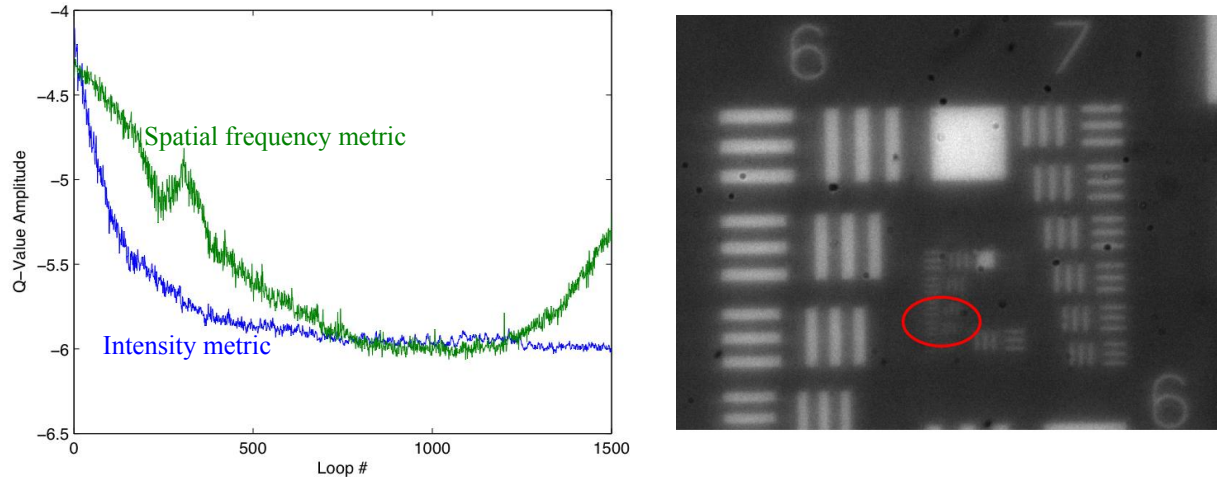


Figure 3: Image quality metric comparison. *Left*: average of three trials each for intensity-based metric control (lower curve) and high spatial frequency based metric control (upper curve). The image intensity metric produced consistently faster and more stable convergence. *Right*: Air Force target image after 1500 iterations with intensity-based metric showing final image resolution of  $\sim 1.38\text{-}1.55\mu\text{m}$ .

### 3.3 Custom calibration target comparison

Three calibration targets were created using high-reflectivity chrome on glass: 1) a grid pattern of  $10\times 10\mu\text{m}$  black (transparent) and white (reflective) squares; 2) a target with larger features consisting of four  $50\mu\text{m}$  diameter reflective circles spaced  $100\mu\text{m}$  apart; 3) a target with  $50\mu\text{m}$  reflective stripes, spaced  $100\mu\text{m}$  apart. The optimization routine was performed using each of the three targets until steady-state image improvement was reached (after 500-1000 iterations for each target). To compare the three targets' performance, after steady state was reached, a custom-made calibration reference object with small features in the shape of figure eights was imaged without readjusting the DM after optimization trials were concluded for each of the calibration targets. The results confirm that calibration targets with uniformly distributed small features allow improved calibration performance.

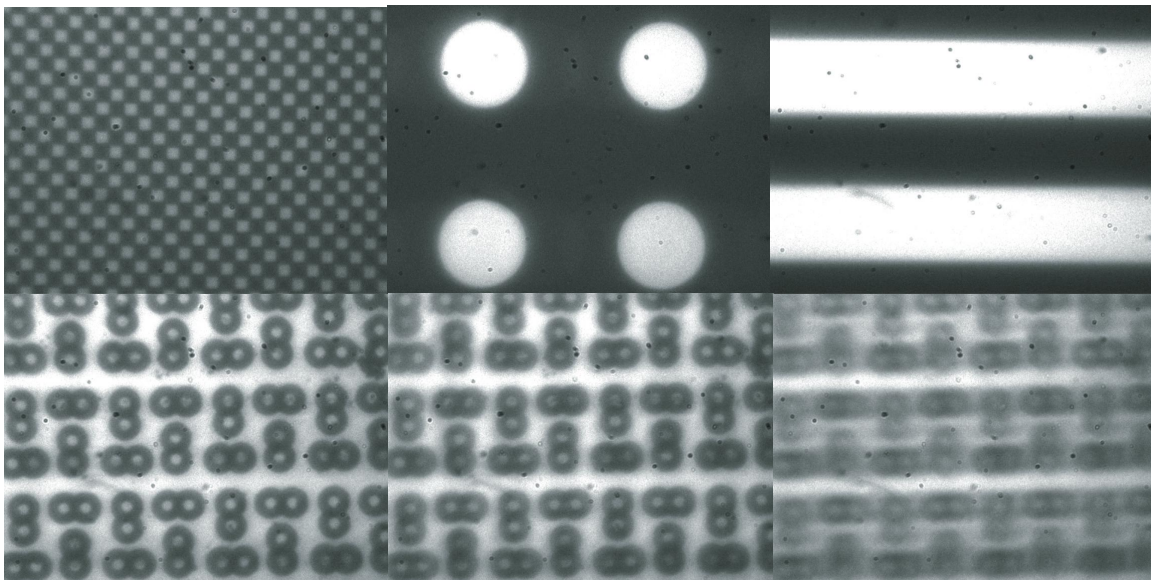


Figure 4: Calibration target comparison. *Top*: Three alternate calibration target patterns used for optimization. *Bottom*: Corresponding images of a reference object when the command vectors obtained during optimization are applied for each of the calibration target trials.

### 3.4 Wavefront sensor measurements

Image quality degradation in the ASOM is directly linked to wavefront errors introduced by aberrations in the scanning lens assembly. In the SPGD calibration method, wavefront aberrations are reduced, but there is no way to know how much of the wavefront error remains after steady state is reached in the controller.

An experiment was performed to measure the wavefront associated with any path through the scanning lens assembly. A Shack Hartmann wavefront sensor (WFS) was placed at the pupil plane of the microscope, just before the imaging camera. A beamsplitter was inserted in the optical path to allow either wavefront sensor based optimization or SPGD optimization. For conventional AO using a WFS, a point source in the object plane is generally used for control, instead of the extended targets that are used in image-based SPGD control. To that end, a 75 $\mu\text{m}$  diameter illumination source (a backlit pinhole) was located at the center of the object plane, replacing the calibration target. Defocus aberrations were introduced by translating the pinhole axially. The system was then controlled using both WFS control and SPGD control.

The resulting images and wavefronts are shown in Figure 5. Both methods produce similar image quality. These results confirm that the SPGD approach is in fact correcting much of the error introduced by aberrations of the scanning lens assembly.

## 4. CONCLUSIONS

Several aspects for the calibration process of the ASOM were evaluated. The use of an SPGD algorithm with intensity as an image sharpness metric provides consistent optimization with 1.5 $\mu\text{m}$  resolution and a convergence in  $\sim 700$  iterations. Zernike based gradient descent control was less successful than individual actuator based control, probably due to sensitivity in optical system alignment. Actuator based SPGD is perhaps more robust since in that approach small misalignments can be compensated during optimization. Although both intensity and spatial frequency can be used as image quality metrics, better performance was obtained with intensity. The best calibration targets were found to be those with small, evenly-distributed features. SPGD optimization and wavefront sensor based direct optimization showed similar results.

## 5. ACKNOWLEDGEMENTS

We are grateful for helpful discussions with Scott Barry of Thorlabs, Inc., Ben Potsaid of Rensselaer Polytechnic Institute, and Jason Stewart and Andrew LeGendre of the Precision Engineering Research Laboratory at Boston University. Deformable mirrors were provided by Boston Micromachines Corporation, and the ASOM instrument was provided by Thorlabs, Inc. Thomas Bifano acknowledges a financial interest in Boston Micromachines Corporation.

## 6. REFERENCES

- [1] Potsaid, B., L.I. Rivera, and J.T. Wen, "Adaptive Scanning Optical Microscope (ASOM): large field of view and high resolution imaging using a MEMS deformable mirror." in Proc. of the SPIE Vol. 6467, 646706-1 - 646706-12, Society of Photo-Optical Instrumentation Engineers, 2007.
- [2] Noll, R.J., "Zernike polynomials and atmospheric turbulence" J. Opt. Soc. Am., Vol. 66, No. 3, March 1976.
- [3] Vorontsov, M.A, and V.P. Sivokon, "Stochastic parallel-gradient-descent technique for high-resolution wave-front phase-distortion correction," Optical Society of America, 2745-2758, 15(10), 1998.
- [4] Muller, R. A., and A. Buffington. "Real-time correction of atmospherically degraded telescope images through image sharpening." Optical Society of America 64, 1200-, 1974.
- [5] Cohen, M., G. Cauwenberghs, M.A. Vorontsov, "Image Sharpness and Beam Focus VLSI Sensors for Adaptive Optics." IEEE Sensors Journal 2(6), 680-690, 2002.
- [6] Murray, L. P., J. C. Dainty, and E. Daly. "Wavefront correction through image sharpness maximization." Proc. of the SPIE Vol. 5823, 40-47, Society of Photo-Optical Instrumentation Engineers, 2005.

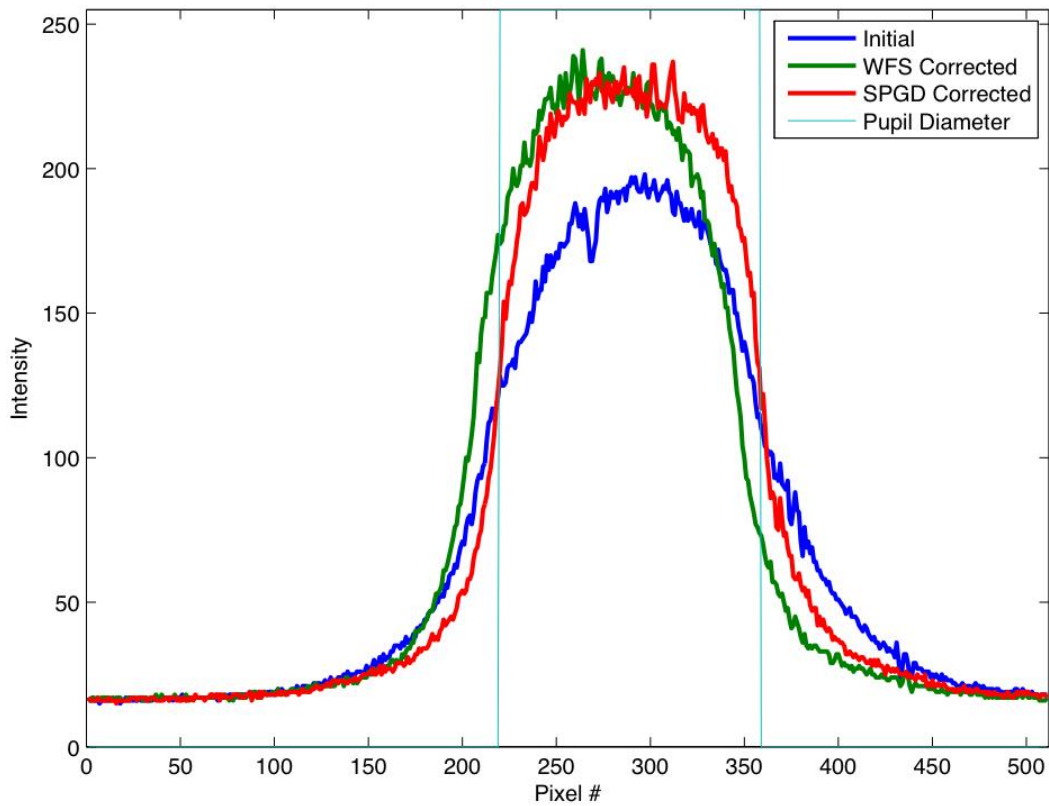
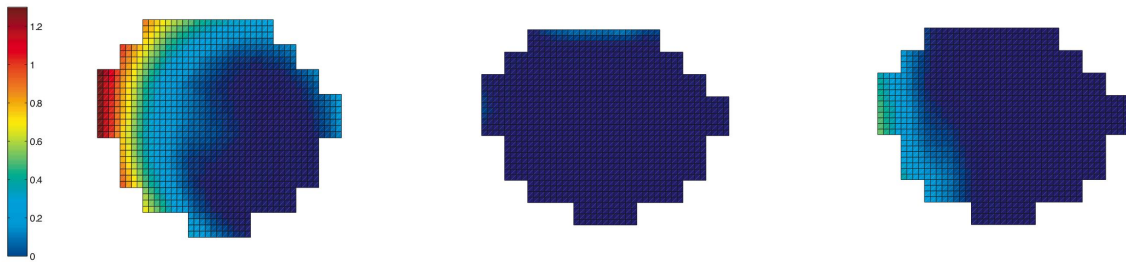
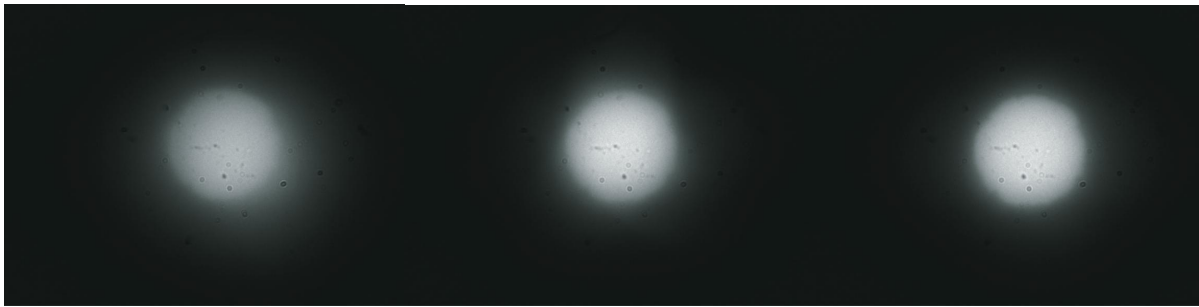


Figure 5: Comparison of wavefront sensor based control results and "sensorless" SPGD control results for an initially defocused illuminated pinhole object. *Top*: Captured images of (left to right) defocused pinhole, WFS corrected pinhole, and SPGD corrected pinhole. *Middle*: Measured wavefront error (left to right) before correction, after correction with WFS, and after correction with SPGD. *Bottom*: Cross sectional intensity measurement across images, showing comparable improvement in image quality, as measured by peak intensity, for both WFS control and SPGD control.